SCIENCE CHINA
Chemistry

•ARTICLES•

October 2025 Vol.68 No.10: 4796–4802
https://doi.org/10.1007/s11426-025-2629-9

A facile ligand engineering strategy to achieve ultra-highly efficient afterglow luminescence of ordinary metal salts

Li Ya Liang[1], Xiao Yuan Wang[1], Ya Ting Gao[1], Da Jun Wu[1], Da Wei Li[1,2*] & Bin Bin Chen[1,2*]

[1]*School of Chemistry & Molecular Engineering, East China University of Science and Technology, Shanghai 200237, China*
[2]*Key Laboratory for Advanced Materials, Shanghai Key Laboratory of Functional Materials Chemistry, Feringa Nobel Prize Scientist Joint Research Center, Frontiers Science Center for Materiobiology & Dynamic Chemistry, East China University of Science and Technology, Shanghai 200237, China*

Received January 6, 2025; accepted March 10, 2025; published online April 21, 2025

Ordinary metal salts have become a promising afterglow material because of the characteristics of wide sources, low cost, and easy availability. However, their extremely weak afterglow efficiency makes them rarely used in practical applications. In this study, we proposed a ligand engineering strategy to greatly enhance the afterglow efficiency of metal salts. $Al_2(SO_4)_3$, as a typical metal salt, has only a photoluminescence quantum yield (PL QY) as low as 0.1% and an unmeasurable phosphorescent QY. After doping with dual organic ligands, the PL QY of $Al_2(SO_4)_3$ has increased by nearly 200 times, reaching 19.90%. Meanwhile, the afterglow intensity of $Al_2(SO_4)_3$ has increased by approximately 20 times, accompanied by a great increase in phosphorescent lifetime from 416.15 to 2870.08 ms (a about 7-time increase). The enhancement mechanism of afterglow efficiency is ascribed to the fact that the excited electrons from the dual ligands can be directly captured by oxygen defects (trap), then transferred to the emitters (Al^{3+} ions), and ultimately achieving efficient afterglow luminescence. This study utilizes ligand engineering strategy to improve the afterglow luminescence efficiency of metal salts, achieving their applications in deep ultraviolet (UV)-excited light emitting devices and visual ethylene glycol recognition.

aluminum sulfate, afterglow luminescence, ligand engineering, light emitting devices, ethylene glycol recognition

Citation: Liang LY, Wang XY, Gao YT, Wu DJ, Li DW, Chen BB. A facile ligand engineering strategy to achieve ultra-highly efficient afterglow luminescence of ordinary metal salts. *Sci China Chem*, 2025, 68: 4796–4802, https://doi.org/10.1007/s11426-025-2629-9

1 Introduction

Ordinary metal salts such as $Al_2(SO_4)_3$ and $MgSO_4$ have been widely discovered to have the ability to emit afterglow luminescence [1,2]. This phenomenon of continuous light emission after switching off the excitation source in metal salts is usually attributed to the electron-trap-associated mechanism [3,4]. Metal salts as a type of common afterglow materials show numerous advantages such as wide sources, low cost, and easy availability. However, compared to other types of inorganic afterglow materials, the afterglow efficiency of metal salts is extremely low, which makes them difficult to be practically applied. To improve afterglow efficiency, most metal salts require rare earth (RE^{3+}) ions doping, combined with high energy ray (X-, γ-, and β-ray) or high-temperature excitation [5,6]. Unfortunately, even with complex structural regulation or harsh excitation conditions, satisfactory afterglow efficiency is still difficult to achieve. Therefore, the development of a new strategy for greatly improving the afterglow efficiency of metal salts is of great significance for broadening their utility across diverse applications, encompassing lighting, display technologies, and sensing domains.

Ligand engineering is an effective strategy for improving the luminescence efficiency of optical materials [7–9]. Using

*Corresponding authors (email: daweili@ecust.edu.cn; binbinchen@ecust.edu.cn)

RE^{3+} ions as a typical example, it is known that the direct excitation of RE^{3+} ions is an inefficient process due to the forbidden 4f transitions [10]. Surprisingly, RE^{3+} ions will emit strong luminescence once they are bound by a suitable organic ligand, which is known as ligand-sensitized luminescence [11–13]. This process involves light absorption of the ligand, intersystem crossing, and the non-radiative energy transfer from the ligand to RE^{3+} ions. Although ligands have achieved great success in sensitizing the luminescence of RE^{3+} ions, their effects on the afterglow luminescence of metal ions have been rarely reported to date.

Herein, a strong ligand engineering strategy is developed to significantly enhance the afterglow efficiency of metal salts (Scheme 1). Pure $Al_2(SO_4)_3$ powder has only one weak afterglow efficiency, with a photoluminescence quantum yield (PL QY) of 0.1% and an unmeasurable phosphorescent QY. After doping with dual organic ligands (tetraphenylethylene (TPE) and 4-carboxyphenylboronic acid (CPBA)), the PL QY of the formed Al^{3+}/TPE/CPBA is significantly increased to 19.90%, nearly 200 times that of $Al_2(SO_4)_3$ and the afterglow intensity is increased by about 20 times. Meanwhile, the lifetime of Al^{3+}/TPE/CPBA is also increased by about 7 times. Because of the remarkable optical characteristics, Al^{3+}/TPE/CPBA are suitable for use in deep ultraviolet-excited light-emitting diodes (DUV-LEDs). Since the luminescence of Al^{3+}/TPE/CPBA has a specific response to ethylene glycol (EG), providing a new method for the visual identification of EG.

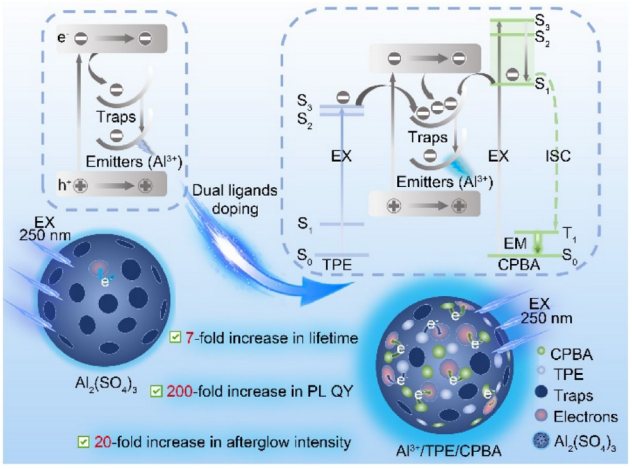

Scheme 1 (Color online) Schematic illustration of ligand-doping strategy enhancing afterglow luminescence of $Al_2(SO_4)_3$.

2 Experimental

2.1 Materials and reagents

CPBA (98%), TPE (98%), and methanol (MeOH, 99.9%) are received from Energy Chemical Co., Ltd. (China). Aluminum sulfate ($Al_2(SO_4)_3$, 99.99%) is purchased from Adamas-beta Reagent Co., Ltd. (China) Terephthalic acid (TPA, 99%) is purchased from Shanghai Macklin Biochemical Technology Co., Ltd. (China). 4-Aminobenzoic acid (PABA, 98%) is obtained from Shanghai J&K Scientific Co., Ltd. (China). Hexaphenylsilole (HPS, 95%), tetrakis(4-aminophenyl) ethene (ETTA, 97%), and ethyl acetate (EA, 99.5%) are purchased from Aladdin Reagent Co., Ltd. (China). Ethanol (EtOH, 95%) is obtained from Shanghai Boer Chemical Reagent Co., Ltd. (China). Dimethyl sulfoxide (DMSO, AR), dichloromethane (DCM, AR), *N*,*N*-dimethylformamide (DMF, AR), and EG (AR) are received from Shanghai Lingfeng Chemical Reagent Co., Ltd. (China). All reagents are dissolved using 18.2 MΩ cm ultrapure water.

2.2 Apparatus

Absorption spectrum is determined by a Lambda 950 UV-visible-near infrared spectrophotometer (PerkinElmer, USA). PL spectra, phosphorescence (phos.) spectra, and phos. lifetimes are measured by an FLS1000 steady state/transient fluorescence spectrometer (Edinburgh Instruments, UK). The decay curve is measured by a HORIBA FluoroMax spectrofluorometer (HORIBA Scientific, Japan). Scanning electron microscopy (SEM) images are obtained by a Helios G4 UC scanning electron microscope (Thermo Fisher Scientific, USA). Elemental mapping is obtained by energy dispersive X-ray spectroscopy (EDS) used in combination with a Helios G4 UC scanning electron microscope. Powder X-ray diffraction (XRD) pattern is determined by an 18KW/D/max2550VB/PC rotating X-ray powder diffractometer (Rigaku Corporation, Japan). X-ray photoelectron spectroscopy (XPS) spectra are analyzed using an ESCALAB 250Xi X-ray photoelectron spectrometer (Thermo Fisher Scientific, USA). Fourier transform infrared (FT-IR) spectra are obtained on a Nicolet6700 FT-IR spectrometer (Thermo Fisher Scientific, USA).

2.3 Synthesis procedure of Al^{3+}/TPE/CPBA

Al^{3+}/TPE/CPBA are synthesized by a facile thermal polymerization treatment of TPE, CPBA, and $Al_2(SO_4)_3$. In detail, $Al_2(SO_4)_3$ solution (1.0 M, 1.6 mL), TPE ethanol solution (0.2 mg/mL, 1.0 mL), and CPBA powder (1.7 mg) are added to a clean screw-neck glass bottle (10 mL) containing 2.4 mL of ultrapure water, and then heated to 120 °C for 300 min. The obtained products are designated as Al^{3+}/TPE/CPBA. To explore the enhancement mechanism of afterglow efficiency, a series of different organic ligands are used for thermal polymerization with $Al_2(SO_4)_3$, following the same synthesis steps as Al^{3+}/TPE/CPBA. The obtained products are designated as Al^{3+}/HPS/CPBA, Al^{3+}/ETTA/CPBA, Al^{3+}/TPE/TPA, and Al^{3+}/TPE/PABA.

2.4 Recognizing procedure of EG

The Al^{3+}/TPE/CPBA powder (0.04 g) is fully dispersed in the different organic solvents (200 μL), including EtOH, DMSO, DCM, EA, DMF, EG, and MeOH. Then, the PL and phos. photographs are taken at an excitation wavelength of 302 nm. Meanwhile, the PL and phos. spectra are tested with the excitation of 300 nm.

To assess the recognition ability of the Al^{3+}/TPE/CPBA for EG in complex environments, simulated industrial EG mixtures are prepared by introducing impurities into AR grade EG. The preparation protocol involves sequentially introducing 0.02 g each of water, acetic acid, formaldehyde, sodium chloride (NaCl, 1 M), and ferric chloride ($FeCl_3$, 1 M) into a 20 mL centrifuge tube, followed by the addition of EG (AR) to achieve a total mass of 10.0 g, resulting in EG mixtures containing 1% impurities. The EG mixtures are thoroughly shaken and mixed, and the recognition process for EG mixtures is maintained identical to that used for EG (AR).

2.5 Theoretical calculation

The energy levels of TPE and CPBA are calculated using Gaussian 16 quantum chemistry software. According to the density functional theory (DFT), the geometry of the ground states of TPE and CPBA are optimized by B3LYP/6-31g (d); then, TD-B3LYP/6-31g (d) method is used to obtain the energy levels of TPE and CPBA molecules, setting charge and spin multiplicity to 0 and 1 to obtain singlet states, 0 and 3 to get triplet states.

3 Results and discussion

To explore the afterglow efficiency enhancement of metal salts by organic ligands, $Al_2(SO_4)_3$ with a weak blue afterglow luminescence is selected as a model metal salt. Meanwhile, TPE (an aggregation-induced emission (AIE) luminogen) and CPBA (a phosphorescent molecule) serve as organic ligands. By the thermal polymerization, Al^{3+}/TPE/CPBA are synthesized (Figure S1, Supporting Information online). The synthesis conditions, including reaction time and temperature, are first investigated. As depicted in Figure S2, the reaction time exhibits only a minor influence on the afterglow performance of the Al^{3+}/TPE/CPBA. In contrast, reaction temperature serves as a more critical parameter in controlling the afterglow characteristics. As shown in Figure S3, a reaction temperature of 120 °C yields optimal afterglow performance, exhibiting both maximum afterglow intensity and prolonged lifetime compared to other synthesis conditions. Consequently, the optimal reaction conditions for synthesizing Al^{3+}/TPE/CPBA are established as 300 min at 120 °C.

The resulting Al^{3+}/TPE/CPBA exhibit an irregular morphology, as evidenced by the SEM image (Figure 1a). Element mapping reveals that the Al^{3+}/TPE/CPBA are predominantly comprised of Al, S, and O as well as minor amounts of B and C, suggesting a homogeneous synthesis because of the uniform element distribution (Figure 1b). Additionally, the XRD pattern of the Al^{3+}/TPE/CPBA largely coincided with those of $Al_2(SO_4)_3$ (Figure 1c), but shows a wider diffraction band compared to $Al_2(SO_4)_3$. This result reveals that $Al_2(SO_4)_3$ is the main component of Al^{3+}/TPE/CPBA, but the doping of dual ligands can disrupt the crystallinity of the $Al_2(SO_4)_3$.

Further structural analysis for Al^{3+}/TPE/CPBA is performed by XPS. High-resolution C 1s spectrum exhibits a typical binding energy at 288.4 eV (Figure 1d), corresponding to carboxyl or carboxylate groups [14,15], which suggests the coordination between CPBA ligands and Al^{3+} ions by Al–O bond. High-resolution O 1s and Al 2p spectra (Figure 1e, f) further reveal the presence of Al–O bond [16,17]. Furthermore, high-resolution S 2p spectrum (Figure 1g) indicates that S is present in the form of sulfate anions, proving the existence of $Al_2(SO_4)_3$. FT-IR spectrum (Figure S4, Supporting Information online) shows that Al^{3+}/TPE/CPBA have three typical peaks at 3063, 1675, and 507 cm^{-1}, corresponding to O–H, C=O, and Al–O, respectively [18]. The similar UV absorption spectra between Al^{3+}/TPE/CPBA and $Al_2(SO_4)_3$ (Figure 1h) clearly reveal that the Al^{3+}/TPE/CPBA are mainly composed of $Al_2(SO_4)_3$, with embedded a small amount of organic ligands inside.

The effect of ligand-doping on the afterglow luminescence of $Al_2(SO_4)_3$ is clearly shown in Figure 2a. Pure $Al_2(SO_4)_3$ powder exhibits an extremely low afterglow intensity, and almost no emission can be observed after the UV lamp is turned off, which is a typical afterglow characteristic of metal salts. After doping with TPE or CPBA, the afterglow efficiency of $Al_2(SO_4)_3$ shows an obvious improvement. Remarkably, the afterglow efficiency of $Al_2(SO_4)_3$ can be maximally enhanced after introducing TPE and CPBA simultaneously. Detailed spectral analysis further reveals the enhancement effect of organic ligands on the afterglow luminescence of $Al_2(SO_4)_3$. As shown in Figure 2b, $Al_2(SO_4)_3$ powder has a blue excitation-independent afterglow emission, with a maximum emission at about 440 nm. After doping with fluorescent TPE ligand (Figure S5), no significant change in the afterglow emission spectra occurs (Figure 2c). Meanwhile, after doping with phosphorescent CPBA ligand, the formed Al^{3+}/CPBA have two afterglow emissions at 424 and 520 nm, respectively (Figure 2d). Because CPBA ligand has a maximum phosphorescent emission at 520 nm (Figure S6), the afterglow emissions of the Al^{3+}/CPBA at 424 and 520 nm should come from $Al_2(SO_4)_3$ and CPBA, respectively. After the formation of the

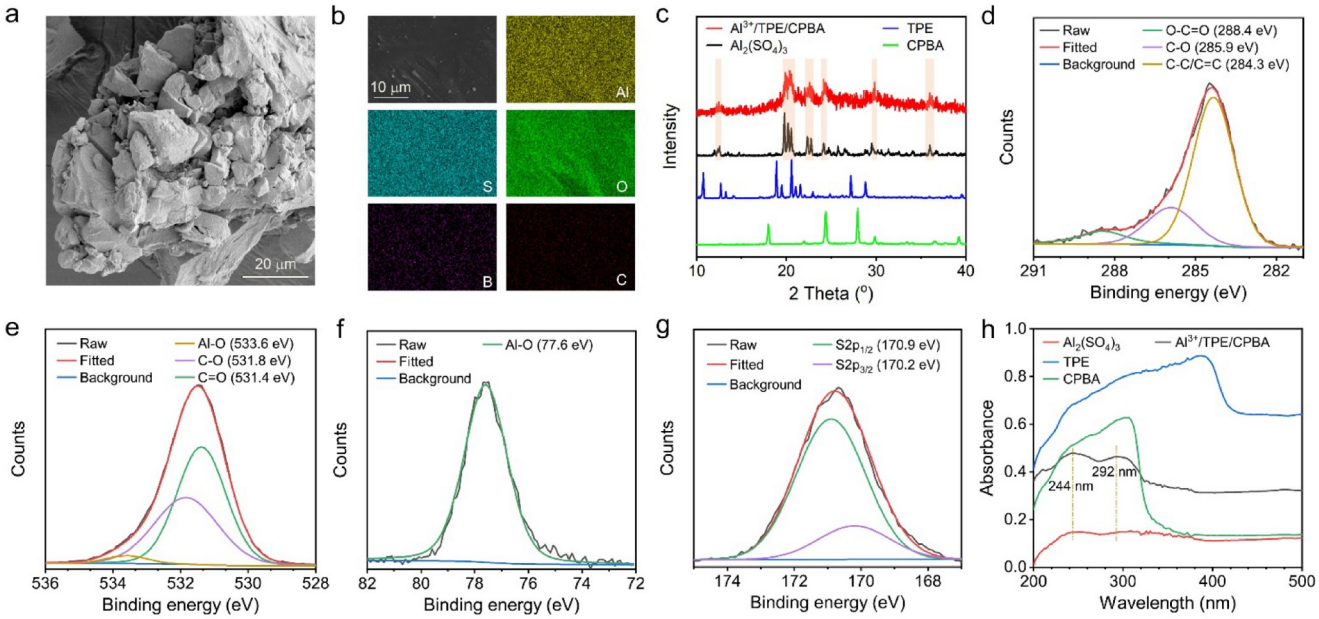

Figure 1 (Color online) Structural characterization of Al^{3+}/TPE/CPBA. (a) SEM image and (b) surface element mapping of Al^{3+}/TPE/CPBA. (c) XRD patterns of Al^{3+}/TPE/CPBA, $Al_2(SO_4)_3$, TPE, and CPBA. (d) High-resolution C 1s spectrum, (e) high-resolution O 1s spectrum, (f) high-resolution Al 2p spectrum, and (g) high-resolution S 2p spectrum of Al^{3+}/TPE/CPBA. (h) Absorption spectra of $Al_2(SO_4)_3$, Al^{3+}/TPE/CPBA, TPE, and CPBA powders.

Al^{3+}/TPE/CPBA, the phosphorescent emission peaks of $Al_2(SO_4)_3$ and CPBA remain (Figure 2e).

According to Figure 2f, after doping with TPE or CPBA, the PL QY of $Al_2(SO_4)_3$ can be increased from 0.1% to 3.90% (Al^{3+}/TPE) and 8.30% (Al^{3+}/CPBA), respectively. When the Al^{3+}/TPE/CPBA is formed, the PL QY greatly increases to 19.90%, achieving an approximately 200 times enhancement. Due to the unmeasurable phosphorescent QY of $Al_2(SO_4)_3$, we have compared the afterglow intensity of $Al_2(SO_4)_3$ before and after ligand doping through pseudo-color analysis of phos. intensity (Figure 2g). Results show that simultaneous doping of TPE and CPBA can achieve up to about 20 times afterglow enhancement, which is significantly higher than doping with TPE alone (9.59-times) or CPBA alone (12.33-times). In addition to the increase in afterglow intensity, ligand doping also achieves a great improvement in afterglow lifetime from 416.15 ms ($Al_2(SO_4)_3$) to 2870.08 ms (Al^{3+}/TPE/CPBA) (Figure 2h).

To prove the universality of the ligand doping strategy for improving the afterglow efficiency of $Al_2(SO_4)_3$, a series of organic ligands have been used, including phosphorescent molecules (TPA and PABA) (Figure S7) and AIE molecules (ETTA and HPS) (Figure S8). All these ligands-doped $Al_2(SO_4)_3$ exhibit enhanced blue afterglow efficiency, although the enhanced efficiency is not as good as the Al^{3+}/TPE/CPBA (Figures S9 and S10), indicating that the afterglow efficiency enhancement of $Al_2(SO_4)_3$ by the developed ligand doping strategy is universal. Compared to conventional rare-earth-doped afterglow materials, although the afterglow performance of the prepared Al^{3+}/TPE/CPBA is not exceptional, their advantages, including simple synthesis (one-step thermal polymerization), mild reaction conditions (120 °C, atmospheric pressure), readily available raw materials, and low production costs, make them have significant industrial application potential.

Furthermore, the enhancement mechanism of the afterglow efficiency of $Al_2(SO_4)_3$ is discussed (Figure 3). As a typical inorganic metal salt, the afterglow luminescence of $Al_2(SO_4)_3$ is attributed to the electron-trap-associated mechanism. Specifically, when the $Al_2(SO_4)_3$ is excited by UV light, the electrons and holes can be generated. The electrons from the valence band (VB) can be promoted to the conduction band (CB) and then be captured by the trap (oxygen defects from SO_4^{2-}). Subsequently, the stored electrons escape gradually from the traps and recombine with emitters (Al^{3+}) by the CB to produce afterglow luminescence [19].

According to the VB-XPS spectrum, the VB of $Al_2(SO_4)_3$ is about 3.10 eV (Figure S11). Considering that the optical bandgap energy of $Al_2(SO_4)_3$ is 1.02 eV measured by the $(ahv)^2$-hv curve (Figure S12), the CB value of $Al_2(SO_4)_3$ can be calculated as 4.12 eV. Meanwhile, by the DFT calculations, the excited singlet states of TPE are 3.02 eV (S_1), 3.59 eV (S_2), and 3.66 eV (S_3), respectively. Although the energy level of the S_1 state of TPE is lower than the VB of $Al_2(SO_4)_3$, according to the result that TPE can greatly improve the afterglow efficiency of $Al_2(SO_4)_3$, suggesting that the excited electrons at higher energy levels can directly be captured by the trap. Similarly, the excited electrons from CPBA can also be captured by the trap while still retaining

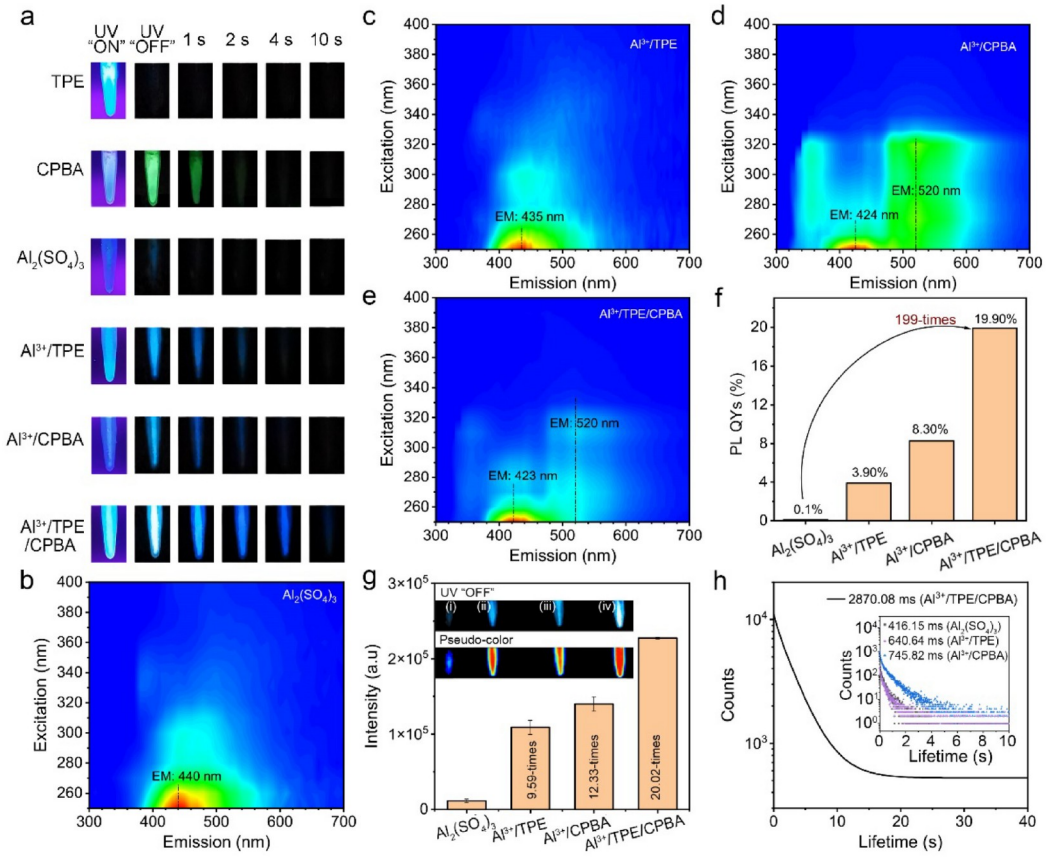

Figure 2 (Color online) The enhancement effect of organic ligands on the afterglow luminescence of $Al_2(SO_4)_3$. (a) Photographs of TPE, CPBA, $Al_2(SO_4)_3$, Al^{3+}/TPE, Al^{3+}/CPBA, and Al^{3+}/TPE/CPBA powders taken before and after removing 302 nm UV light. 3D phos. spectra of (b) $Al_2(SO_4)_3$, (c) Al^{3+}/TPE, (d) Al^{3+}/CPBA, and (e) Al^{3+}/TPE/CPBA. (f) PL QYs of $Al_2(SO_4)_3$, Al^{3+}/TPE, Al^{3+}/CPBA, and Al^{3+}/TPE/CPBA. (g) Afterglow intensity of $Al_2(SO_4)_3$, Al^{3+}/TPE, Al^{3+}/CPBA, and Al^{3+}/TPE/CPBA (inset: afterglow photographs and pseudocolor analysis of (i) $Al_2(SO_4)_3$, (ii) Al^{3+}/TPE, (iii) Al^{3+}/CPBA, and (iv) Al^{3+}/TPE/CPBA.). The afterglow intensity values are obtained by pseudocolor analysis. (h) Phos. lifetimes of Al^{3+}/TPE/CPBA (inset: phos. lifetimes of $Al_2(SO_4)_3$, Al^{3+}/TPE, and Al^{3+}/CPBA.). Delay time: 2 ms.

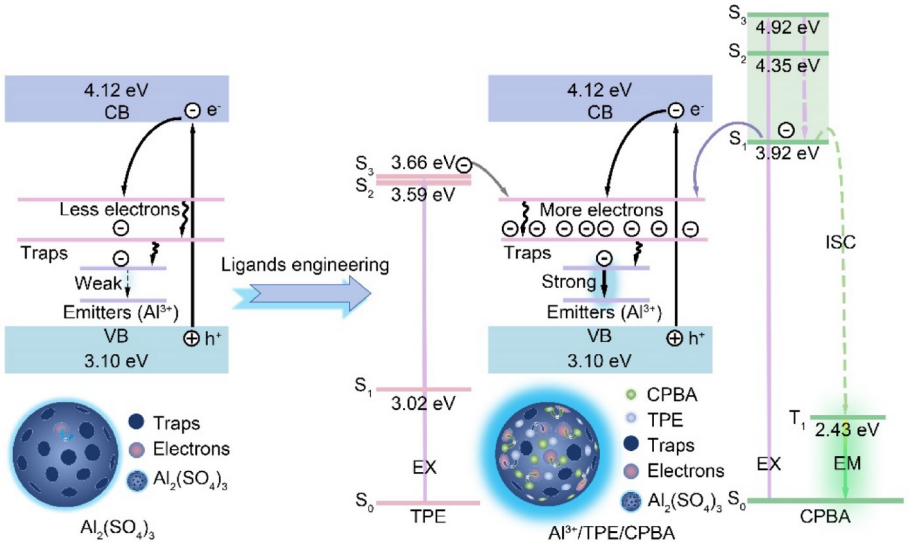

Figure 3 (Color online) The possible migration pathways of the excited electrons in $Al_2(SO_4)_3$ and Al^{3+}/TPE/CPBA.

their original phos. emission (520 nm). Consequently, upon the formation of the Al^{3+}/TPE/CPBA, the excited electrons from both TPE and CPBA are effectively captured by the trap centers. This increased electron population in the traps

leads to enhanced afterglow intensity and prolonged afterglow lifetime following the cessation of light excitation.

Variable-temperature phos. spectra further confirm the ligand-enhanced defect luminescence. As shown in Figure S13, the afterglow intensity of Al^{3+}/TPE/CPBA remains relatively stable below 300 K, but undergoes significant thermal quenching when the temperature exceeds this threshold. This is because the electrons captured by $Al_2(SO_4)_3$ defects originate from organic ligands, and at elevated temperatures (>300 K), intense molecular motion greatly promotes non-radiative recombination pathways. This significantly reduces the probability of excited electrons of ligands being captured by defects, resulting in a decrease in the afterglow intensity of the Al^{3+}/TPE/CPBA.

Because of the excellent afterglow luminescence, Al^{3+}/TPE/CPBA have a high potential for use in DUV-LEDs. As shown in Figure 4a, the prepared DUV-LEDs emit bright white light by using 250 nm UV chips. As the driving current rises from 50 to 300 mA, the emission intensities of the DUV-LEDs improve gradually (Figure 4b). Notably, the chromaticity coordinates, color rendering index, and color purity of the DUV-LEDs have only negligible variations with changes in the driving current, showing the highly stable of DUV-LEDs (Figure 4c and Table S1 , Supporting Information online). These observations underscore the significant potential of Al^{3+}/TPE/CPBA in the advancement of novel DUV-LEDs technology.

EG possesses significant toxicity, posing risks to both animals and humans [20,21]. Specific identification of EG facilitates the monitoring of environmental contamination and prevents leaks and ingestion during industrial applications, thereby safeguarding the health of workers and the public [22]. Remarkably, Al^{3+}/TPE/CPBA offer a promising solution for EG identification. As shown in Figure 4d, when Al^{3+}/TPE/CPBA powder is dispersed in different organic solvents (EG, MeOH, EtOH, EA, DMSO, DCM, and DMF), the Al^{3+}/TPE/CPBA show bright blue PL under UV excitation only in an EG solution. From the PL spectra (Figure 4e), it can be seen that except for EG, all other organic solvents can effectively quench the PL of the Al^{3+}/TPE/CPBA, thereby achieving the visual recognition of EG. Meanwhile, only when the Al^{3+}/TPE/CPBA are dispersed in EG and DCM, they exhibit two afterglow emissions at about 433 and 484 nm, respectively (Figure 4f), providing a phosphorescent channel for detecting EG. The EG-responsive afterglow luminescence should be attributed to the differences in a dissolution of three components of Al^{3+}/TPE/CPBA in different solvents. Furthermore, we have evaluated the ability of Al^{3+}/TPE/CPBA for EG recognition in complex environments. Comparative analysis of the spectral data obtained from EG (AR) and EG mixtures containing 1% impurities reveals that the presence of these impurities has a negligible impact on the EG recognition capability of Al^{3+}/ TPE/CPBA (Figure S14), suggesting a promising practical application potential.

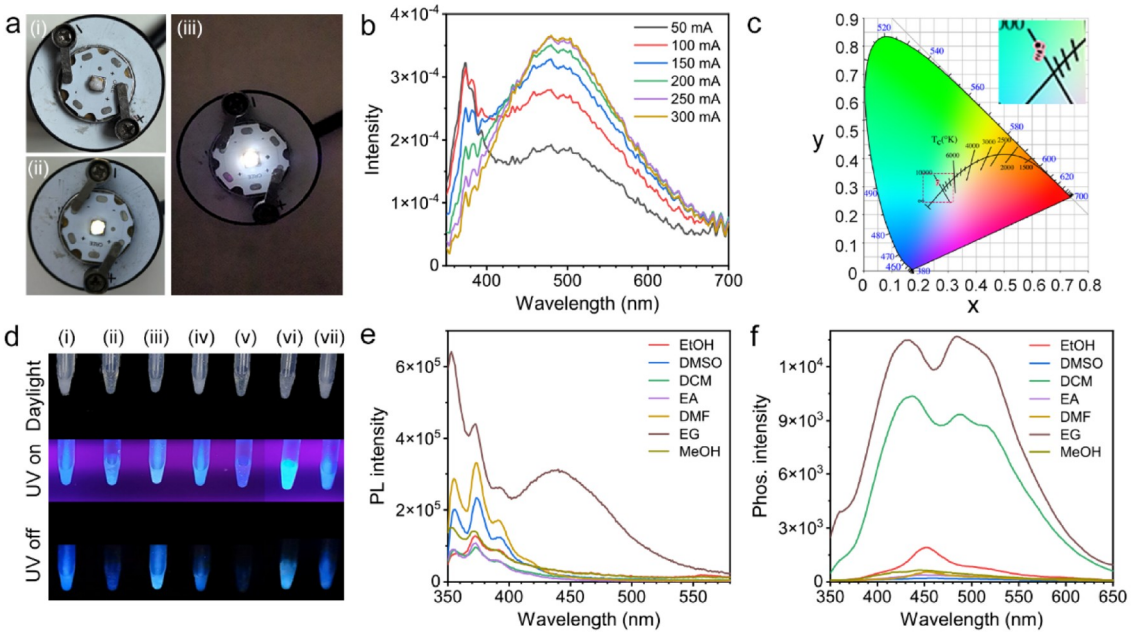

Figure 4 (Color online) Versatile applications of the Al^{3+}/TPE/CPBA. (a) Photographs of the as-fabricated DUV-LEDs lighted one. (b) The emission spectra of DUV-LEDs device under different drive currents. Excitation: 250 nm. (c) The chromaticity coordinates of DUV-LEDs under different drive currents in CIE 1931 color spaces (inset: a magnified area marked with an orange square in color spaces.). (d) Photographs of Al^{3+}/TPE/CPBA powder (40 mg) upon treatment on different organic solvents (200 μL) taken before and after removing 302 nm UV light. Organic solvents include (i) EtOH, (ii) DMSO, (iii) DCM, (iv) EA, (v) DMF, (vi) EG, and (vii) MeOH. (e) PL and (f) phos. spectra of Al^{3+}/TPE/CPBA after the treatment with different organic solvents. Excitation : 300 nm. Delay time: 2 ms.

4 Conclusions

In conclusion, a powerful ligand engineering strategy is developed for greatly enhancing the afterglow efficiency of $Al_2(SO_4)_3$. The doping of organic ligands simultaneously enhances the afterglow intensity and lifetime of $Al_2(SO_4)_3$. The ligand-enhanced afterglow luminescence is proven to be attributed to the fact that more electrons (from the excited electrons of the ligands) can be captured by the trap, and then transferred to the emitters, thereby achieving efficient afterglow luminescence. To the best of our knowledge, this is the first case of organic ligands enhancing the afterglow luminescence of metal ions. This work not only provides the possibility for designing and preparing metal salts with ultra-highly efficient afterglow luminescence, but also is of great significance for understanding the dynamics of excited state electrons in organic-inorganic afterglow materials.

Acknowledgements This work was supported by the National Natural Science Foundation of China (22176058), the Science and Technology Commission of Shanghai Municipality (24DX1400200, 22ZR1416800, 23ZR1416100), the Program of Introducing Talents of Discipline to Universities (B16017), and the Fundamental Research Funds for the Central Universities (222201717003). We thank the Research Center of Analysis and Test of East China University of Science and Technology for help with the characterization.

Conflict of interest The authors declare no conflict of interest.

Supporting information The supporting information is available online at http://chem.scichina.com and http://link.springer.com/journal/11426. The supporting materials are published as submitted, without typesetting or editing. The responsibility for scientific accuracy and content remains entirely with the authors.

1 Liang LY, Gao YT, Chang S, Lv J, Wang L, Liu ML, Wu DJ, Ye MJ, Chen BB, Li DW. *Adv Opt Mater*, 2024, 12: 2401642
2 Liang LY, Chen BB, Wang Y, Gao YT, Chang S, Liu ML, Li DW. *J Colloid Interface Sci*, 2023, 649: 445–455
3 Yang L, Gai S, Ding H, Yang D, Feng L, Yang P. *Adv Opt Mater*, 2023, 11: 2202382
4 Wei ZJ, Yin C, Sun M, Long K, Zhang Z, Yan Z, Wang W, Yuan Z. *ACS Appl Mater Interfaces*, 2024, 16: acsami.4c00531
5 Lakshmanan AR. *Prog Mater Sci*, 1999, 44: 1–187
6 Gupta SK, Sudarshan K, Modak B, Yadav AK, Modak P, Jha SN, Bhattacharyya D. *J Phys Chem C*, 2020, 124: 16090–16101
7 Kumawat NK, Swarnkar A, Nag A, Kabra D. *J Phys Chem C*, 2018, 122: 13767–13773
8 Shen Z, Zhao S, Song D, Xu Z, Qiao B, Song P, Bai Q, Cao J, Zhang G, Swelm W. *Small*, 2020, 16: 1907089
9 Zhu X, Zhang H, Zhang F. *ACS Mater Lett*, 2022, 4: 1815–1830
10 Gai S, Li C, Yang P, Lin J. *Chem Rev*, 2014, 114: 2343–2389
11 Zhao Y, Gu S, Xu S, Wang L. *Anal Chem*, 2021, 93: 14317–14322
12 Moore EG, Samuel APS, Raymond KN. *Acc Chem Res*, 2009, 42: 542–552
13 Chen BB, Liu ML, Zhan L, Li CM, Huang CZ. *Anal Chem*, 2018, 90: 4003–4009
14 Cai W, Gao H, Chu C, Wang X, Wang J, Zhang P, Lin G, Li W, Liu G, Chen X. *ACS Appl Mater Interfaces*, 2017, 9: 2040–2051
15 Yang X, Yan D. *Adv Opt Mater*, 2016, 4: 897–905
16 Zhang Q, Wang G, Li X, Chang Y, Liu W, Wu Z, Bi S, Zhan H. *Catal Lett*, 2024, 154: 270–279
17 Wang X, Yao P, Li Y, Zhou H, Xiao Y, Deng M, Kang L, Zhou P. *Tribol Int*, 2023, 179: 107960
18 Zawrah MF, Ghanaym EE, Sadek HEH, El Defrawy SA, Ali OAM. *Ceramics Int*, 2019, 45: 17598–17610
19 Yang L, Gai S, Ding H, Yang D, Feng L, Yang P. *Adv Opt Mater*, 2023, 11: 2370038
20 Hess R, Bartels MJ, Pottenger LH. *Arch Toxicol*, 2004, 78: 671–680
21 Moore MM, Kanekar SG, Dhamija R. *Radiol Case Rep*, 2008, 3: 122
22 Fowles J, Banton M, Klapacz J, Shen H. *Toxicol Lett*, 2017, 278: 66–83